Title

LES investigation of a Passively Excited Impinging Jet

Authors

Uddin, Naseem
Neumann, Sven Olaf
Weigand, Bernhard
et al.

Publication Date

2021-02-01

DOI

10.1016/j.ijheatmasstransfer.2020.120705

International Journal of Heat and Mass Transfer 165 (2021) 120705

Contents lists available at ScienceDirect

International Journal of Heat and Mass Transfer

journal homepage: www.elsevier.com/locate/hmt

LES investigation of a Passively Excited Impinging Jet

Naseem Uddin[a,*], Sven Olaf Neumann[b], Bernhard Weigand[c], Bassam A. Younis[d]

[a] Universiti Teknologi Brunei, Jalan Tungku Link, Gadong, BE1410, Brunei Darussalam
[b] Fachhochschule Kiel, Grenzstraße 3, Kiel 24149, Germany
[c] Institut für Thermodynamik der Luft- und Raumfahrt, Universität Stuttgart, Pfaffenwaldring 31, Stuttgart 70569, Germany
[d] Department of Civil & Environmental Engineering, University of California, Davis, California, USA

ARTICLE INFO

Article history:
Received 22 July 2020
Revised 20 October 2020
Accepted 8 November 2020
Available online 25 November 2020

Keywords:
Periodic flow
passive excitation
jet impingement
Large Eddy Simulations
Heat Transfer

ABSTRACT

Periodic vortex shedding which forms when fluid moves over a circular cylinder creates a wake which causes fluctuating unsteady forces on structures. The oscillating wake may also serve to enhance heat transfer rates from a surface on which it impinges. In this paper we investigate the passive excitation of the impinging jet's velocity field using a cylindrical insert. The insert is placed just before where the jet issues from the circular pipe. The flow is examined using Large Eddy Simulations (LES). The jet's Reynolds number based on bulk inlet velocity is 23,000 and jet's outlet-to-target wall distance is two. It is found that using a cylindrical insert in the impingement pipe results in enhanced heat transfer rates for cooling applications.

1. Introduction

The behaviour of impinging jets has been investigated in depth both numerically and experimentally in the past. Excellent reviews of the state of art can be found in [1–3]. The core target of the present study is on the use of passively-generated excitations to augment the heat-transfer rates from the impinging jet–a topic that has received little attention to date with the focus, so far, being mainly directed towards the study of the effects of excitation by means of active control [4–7]. While such methods have proved to be effective in the enhancement of heat-transfer rates, their use requires an efficiently devised mechanism for the control of the flow field and their efficiency depends heavily on the amplitude of the excitation and judicious choice of frequencies. Passive excitation of the jet, on the other hand, can potentially produce similar benefits with far less complexity and cost.

Despite its potential benefits, there are only but a few studies focused on passive jet excitation and its influence on the target wall heat transfer. Herwig et al. [8] investigated the impinging jet heat transfer variability due to unsteadiness introduced through a circular ring installed in free jet that has generated periodic vortex shedding. This leads to precessing effect and intricate flow pattern as flow moves around circular ring. They found that the heat transfer can be augmented for the von Karman jet nozzle in which additional unsteadiness and turbulence is introduced. Haneda et al. [9] explored a setup in which a circular cylinder elastically suspended with a cantilever-type plate spring in the slot jet impingement region. The cylinder was 3 or 5 times as large as the jet slot width whereas slot jet's Reynolds number is from 10,000 to 5,000. Gao et al [10] used arrays of triangular tabs installed on the exit of turbulent round impinging jets issuing from a long pipe. They found that for small nozzle-to-plate spacings the locally heat transfer can be increased up to 25% compared with the case of no tabs installed. Also, the first and secondary peaks in radial distribution of the Nusselt number are observed at jet's outlet-to-target wall distance of 4.

The control of vortex shedding by a cylinder has been the subject of several studies using a feedback mechanism, surface modifications or cylinder oscillations. The wake from a cylinder can be an effective mean for increasing heat transfer at target wall. Bhattacharya and Ahmed [11] conducted experiments to measure mean surface pressures and heat transfer rates on a flat plate with jet impingement of Reynolds number =50,000. Four cases were considered for the passive excitation of the jet consisting of (1) in-line jet, (2) in-line jet with stationary cylinder placed at 1.5D from jet's outlet, (3) in-line jet with eccentrically mounted oscillating cylinder, and (4) in-line jet with oscillating cambered airfoil. It was found that enhancement of the heat transfer rates can be achieved which is attributed to enhanced mixing/turbulence due to wakes vortex dynamics and oscillatory dislocation of the stagnation streamline. In terms of excitation device stationary cylinder

* Corresponding author. Universiti Teknologi Brunei, Jalan Tungku Link, Gadong, BE1410, Brunei Darussalam.
E-mail address: naseem.uddin@utb.edu.bn (N. Uddin).

https://doi.org/10.1016/j.ijheatmasstransfer.2020.120705
0017-9310/

Nomenclature

D	diameter of jet, m
d	diameter of insert, m
H	jet's outlet to the target wall distance, m
h	convective heat transfer coefficient, W/m^2K
k	turbulent kinetic energy, m^2/s^2
K	constant convection velocity, m/s
κ	wavenumber, 1/m
Lp	delivery pipe length, m
q''_w	heat flux at wall, W/m^2
r	radius, m
R_{uu}	autocorrelation of velocity signal
L(t)	integral length scale, m
U_b	Bulk velocity at jet's inlet, m/s
U	Mean velocity in walljet region, m/s
<u>	radial component of velocity, m/s
u_τ	frictional velocity, m/s
u+	dimensionless turbulent velocity in wall bounded flows u/ uτ
y+	dimensionless wall coordinates Δy.uτ/ν,
P	Pressure, Pa
T	Temperature, K

Greek

$\hat{\phi}$	large scale component
$\tilde{\phi}$	Subgrid component
ν	kinematic viscosity
Γ_s	subgrid thermal diffusivity
λ	Thermal conductivity, W/mK

Turbulent fluctuations

$\overline{u'v'}$	turbulent shear stress
$\overline{u'u'}$, $\overline{v'v'}$, $\overline{w'w'}$	turbulent velocity fluctuations
$\overline{T'T'}$	turbulent temperature fluctuations

Dimensionless Numbers

Re	Reynolds number U_bD/ν
Pr	Prandtl number
Pr_s	subgrid turbulent Prandtl number
Nu	Nusselt number
Re_{hD}	$U_{max}D_h/\nu$

and oscillating cylinder heat transfer on target wall results were not very different.

Li et al. [12] presented heat transfer results of large eddy simulation (LES) of normally impinging elliptic air-jet heat transfer at a Reynolds number of 4,400, with an orifice-to-plate distance fixed to be 5 in the unit of the jet nozzle effective diameter. LES are carried out using a dynamic subgrid model and Open-FOAM. Natarajan et al. [13] presented large eddy simulation for jet impingement with a vibrating wall. The jet's Reynolds number was 23,000 and the jet's outlet-to-target wall was two diameters. Vortical structures are shown to play a major role in convective heat transfer even under the vibrating conditions of the impingement wall. Krumbein et al. [14] investigated slot jet impingement at a moderate Reynolds number of 9,120, using a time-accurate Very Large Eddy Simulation (VLES). The results were compared with experimental data. Penumadu and Rao [15] conducted LES simulations to get a better understanding of the flow physics in multiple jet impingement arrays. The Reynolds number was varied from 5,000 to 90,000. They found that CFD is over-predicting the pressure drop in case of multiple jet impingement as high as 50%.

In this paper a case of passive excitation of the impinging jet's velocity field has been investigated. The excitation is produced using a cylinder which is inserted just before the jet emerges from the pipe. The flow is studied numerically using Large Eddy Simulations (LES). The jet's Reynolds number ($Re=U_bD/\nu$) of the main pipe flow is 23000 and the dimensionless jet's outlet-to-target wall distance (H/D) is two. The benchmark test case of single jet impingement (Cooper et al. [16]) is investigated for comparative purpose. The interested reader is referred to Uddin et al. [17] for the discussion on the case of natural jet impingement without an insert.

An impinging jet can be excited actively by modulating jet's velocity and temperature fields in time. Also a jet can be excited passively by placing insert inside the pipe or fee jet development zone before it impinges on the surface. In the present study the focus is set on passive excitation using a cylindrical insert, which is placed just before the jet's issues from a pipe.

2. Governing Equations

In LES, the quantities are divided into a large-scale and a small-scale motions as $\phi = \hat{\phi} + \tilde{\phi}$. Here, ϕ serve as the flow quantities like velocity (u_i), pressure (p), temperature (T) etc. The quantity $\hat{\phi}$ serve as the large scale (resolved) component which is time dependent, and the quantity $\tilde{\phi}$ denotes the small scale (unresolved), or sub-grid component. Here in this paper an implicit filtering approach is used i.e. the grid size is use as appropriate filter. For Newtonian fluids with no body forces and sub-grid scale density fluctuations we can write conservation equations as follows (Pope [18]):

$$\frac{\partial \rho}{\partial t} + \frac{\partial (\rho \hat{u}_i)}{\partial x_i} = 0 \tag{1}$$

$$\frac{\partial (\rho \hat{u}_i)}{\partial t} + \frac{\partial (\rho \hat{u}_i \hat{u}_j)}{\partial x_j} = \frac{\partial}{\partial x_j}\left\{\mu\left[\frac{\partial \hat{u}_i}{\partial x_j} + \frac{\partial \hat{u}_j}{\partial x_i}\right]\right\} - \frac{\partial \tau_{ij}^{sgs}}{\partial x_j} - \frac{\partial \hat{p}}{\partial x_i} \tag{2}$$

Stresses at sub-grid level are modelled as (Pope [9]):

$$\tau_{ij}^{sgs} - \frac{1}{3}\delta_{ij}\tau_{kk}^{sgs} = -2\mu_s\left[\hat{S}_{ij} - \frac{1}{3}\delta_{ij}\hat{S}_{kk}\right] \tag{3}$$

Where μ_s is the subgrid viscosity defined as $\mu_s = \rho(c_s\Delta)^2\widehat{S}$, where c_s is dynamically adjusted based on dynamic Smagorinsky model proposed by Germano et al. [19] . After filtering operation, the energy equation can also be expressed as:

$$\frac{\partial (\rho c_p \hat{T})}{\partial t} + \frac{\partial (\rho c_p \hat{u}_j \hat{T})}{\partial x_j} = \frac{\partial}{\partial x_j}\left[\Gamma c_p \frac{\partial \hat{T}}{\partial x_j}\right] - \frac{\partial q_j^{sgs}}{\partial x_j} \tag{4}$$

The turbulent heat-fluxes at sub-grid level are specified by using the gradient diffusion assumption as:

$$q_j^{sgs} = -\Gamma_s c_p \frac{\partial \hat{T}}{\partial x_j} \tag{5}$$

where, $\hat{T}$ is the resolved temperature and Γ_s is the subgrid thermal diffusivity. After substituting eq. (5) into eq. (4) the following form of the energy equation is obtained:

$$\frac{\partial (\rho c_p \hat{T})}{\partial t} + \frac{\partial (\rho c_p \hat{u}_j \hat{T})}{\partial x_j} = \frac{\partial}{\partial x_j}\left[(\Gamma + \Gamma_s) c_p \frac{\partial \hat{T}}{\partial x_j}\right] \tag{6}$$

The sub-grid thermal diffusivity Γ_s can be expressed as

$$\Gamma_s = \mu_s / Pr_s \tag{7}$$

where Pr_s is the sub-grid turbulent Prandtl number which is set to 0.9 (Uddin et al. [17]). The values assigned to the subgrid turbulent Prandtl number are ranging form 0.3 to 0.9. But more and more researcher have taken a value of 0.9. Deardorff [20,21] used a subgrid Prandtl number less than one. Moeng and Wyngaard [22] used a value of 0.4 for subgrid Prandtl number, Gao et al. [23] used a

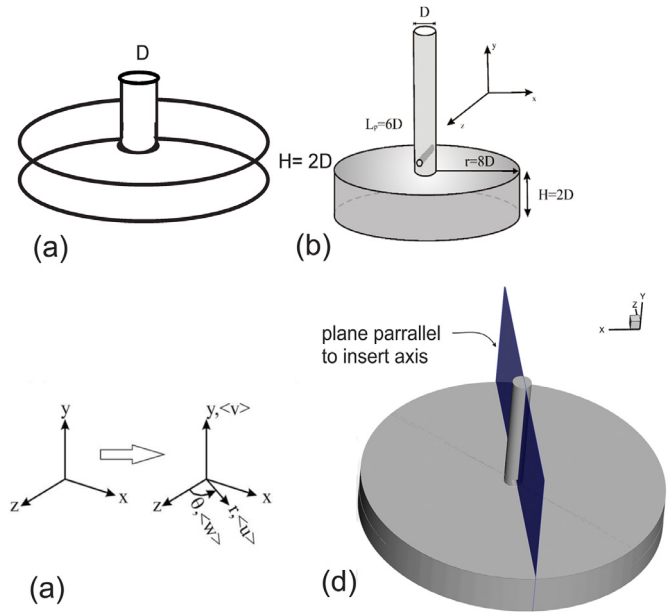

Figure 1. (a) Computational domain without insert (b) Computational domain with insert (c) the Cartesian coordinate used for the computations and the cylindrical domain. (d) Plane parallel to insert axis

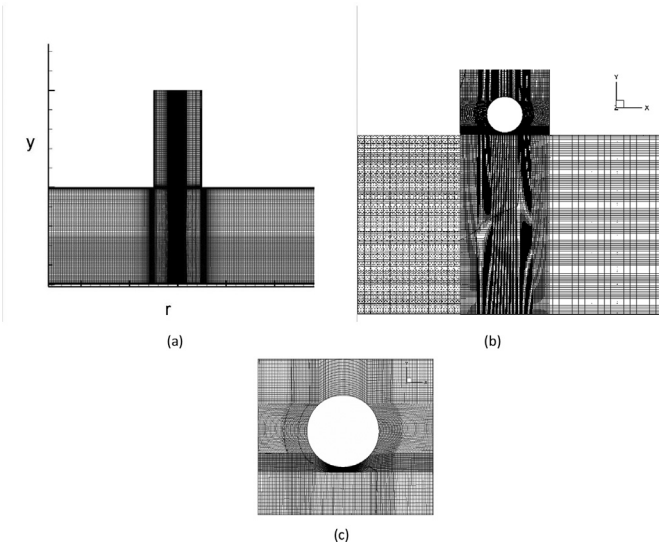

Figure 2. Cross section of grids used for (a) natural jet impingement (b) jet impingement with cylindrical insert and (c) close-up view of grid around insert.

value of 0.3 for subgrid Prandtl number. More recently, Hadziabdic [24] simulated a quarter of an impinging jet using LES with value of subgrid Prandtl number of 0.9. From our previous LES of impingement of natural jet studies, we found that a value of 0.9 is giving good results. As current case is also a jet impingement case the same 0.9 value is selected.

The test filtering has been done by averaging over 27 control volumes. The above equations are solved with the density taken as constant.

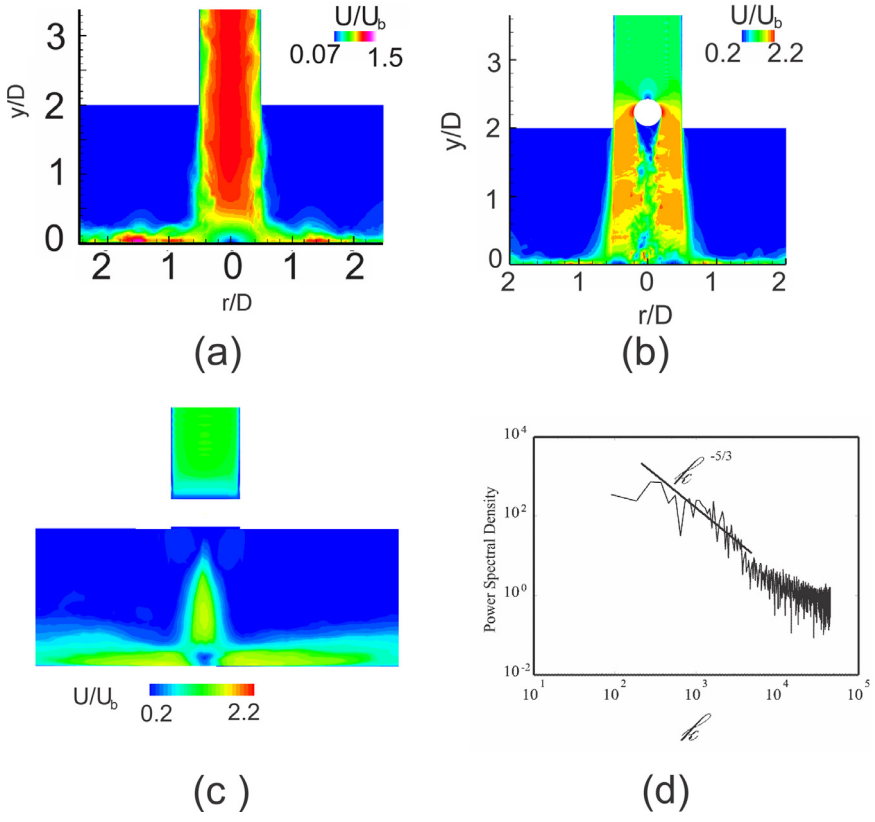

Figure 3. Instantaneous Velocity distribution in the jet and in the impingement region (a) without insert (b) Time averaged mean velocity (b) in perpendicular to cross-section of cylinder (c) in transverse direction of cylinder (parallel to the axis of insert). Flow over a cylindrical insert and formation of a twin jet system can be observed (d) The velocity distribution at the pipe outlet with and without insert. (b) Power Spectral density (PSD) of velocity fluctuations in the jet at y/D=1 and r/D=0.5, the line indicates the slope of the inertial subrange.

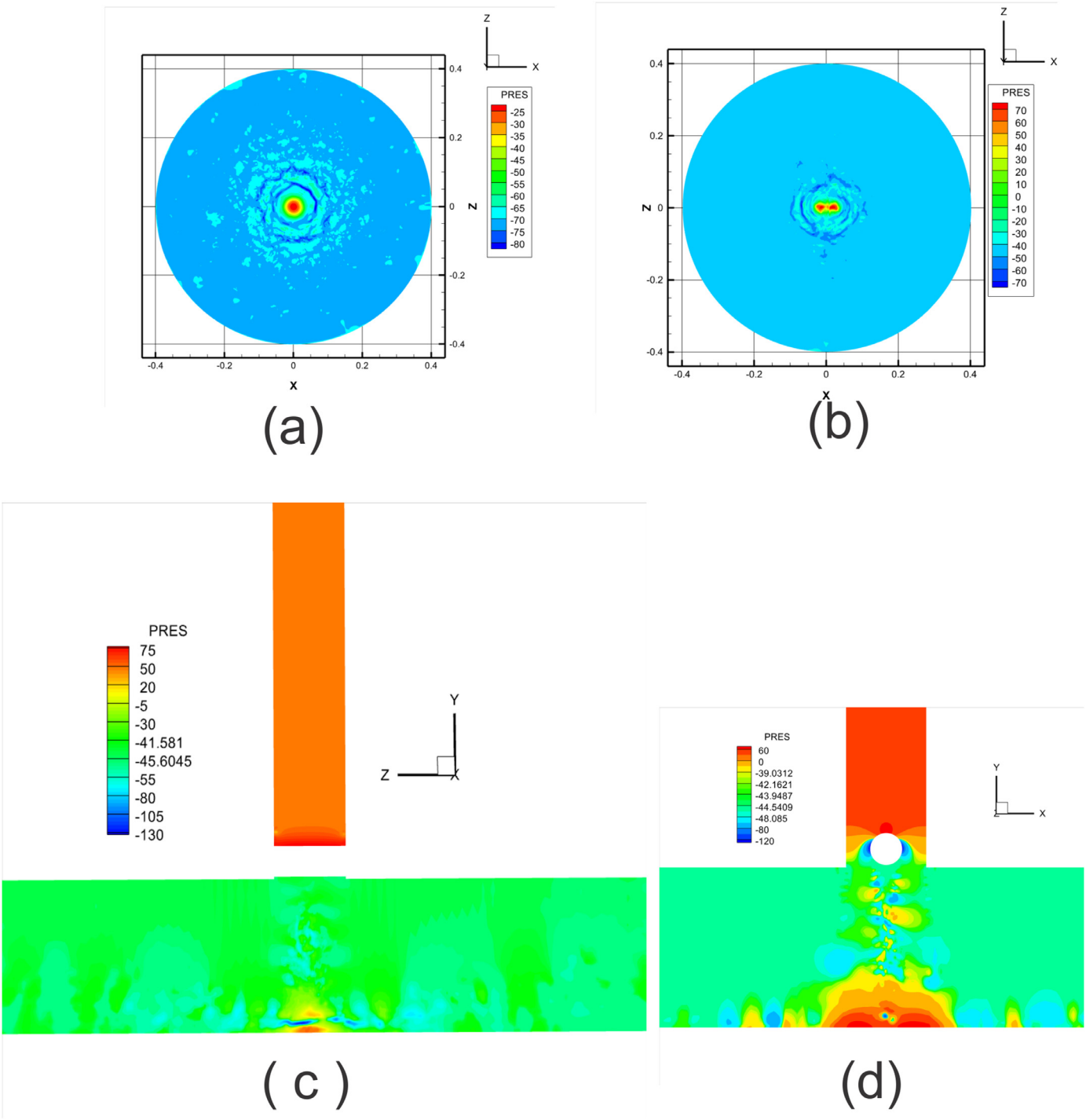

Figure 4. Instantaneous pressure distribution (a) at the target wall for no insert case (b) close to target wall perpendicular to the cross-section of the cylinder (c) in transverse direction of the cylinder (parallel to the axis of insert) (d) perpendicular to the cylinder

3. Inflow and Boundary Conditions

The mean velocity profile of a hydrodynamically fully developed turbulent pipe flow, together with time-varying velocity fluctuations, are prescribed at the inlet plane (see Fig. 1). The turbulent mean velocity profile for a fully developed pipe flow is prescribed from Kays et al. [25]:

$$u^+ = 2.5 \ln\left[\frac{1.5y^+(1 + r/(D/2))}{1 + 2(r/(D/2))^2}\right] + 5.5 \quad (8)$$

where, $y^+ = \Delta y\ u_\tau/\nu$ represents the pipe wall normal direction, D is the diameter of the pipe, u^+ is dimensionless wall velocity is $u^+ = u/u_\tau$. In case of a natural jet (non-excited jet), the bulk inlet velocity (U_b) is calculated from equation (8). The above equation needs the correct estimate of frictional velocity which is estimated from a smooth pipe friction correlation (see e.g. White [26]).

The appropriate generation of turbulent inflow fluctuations was done using the artificial turbulence generation procedure devised by Klein et al. [27]. According to this approach the digital filter is applied on random data and velocity fluctuations are gen-

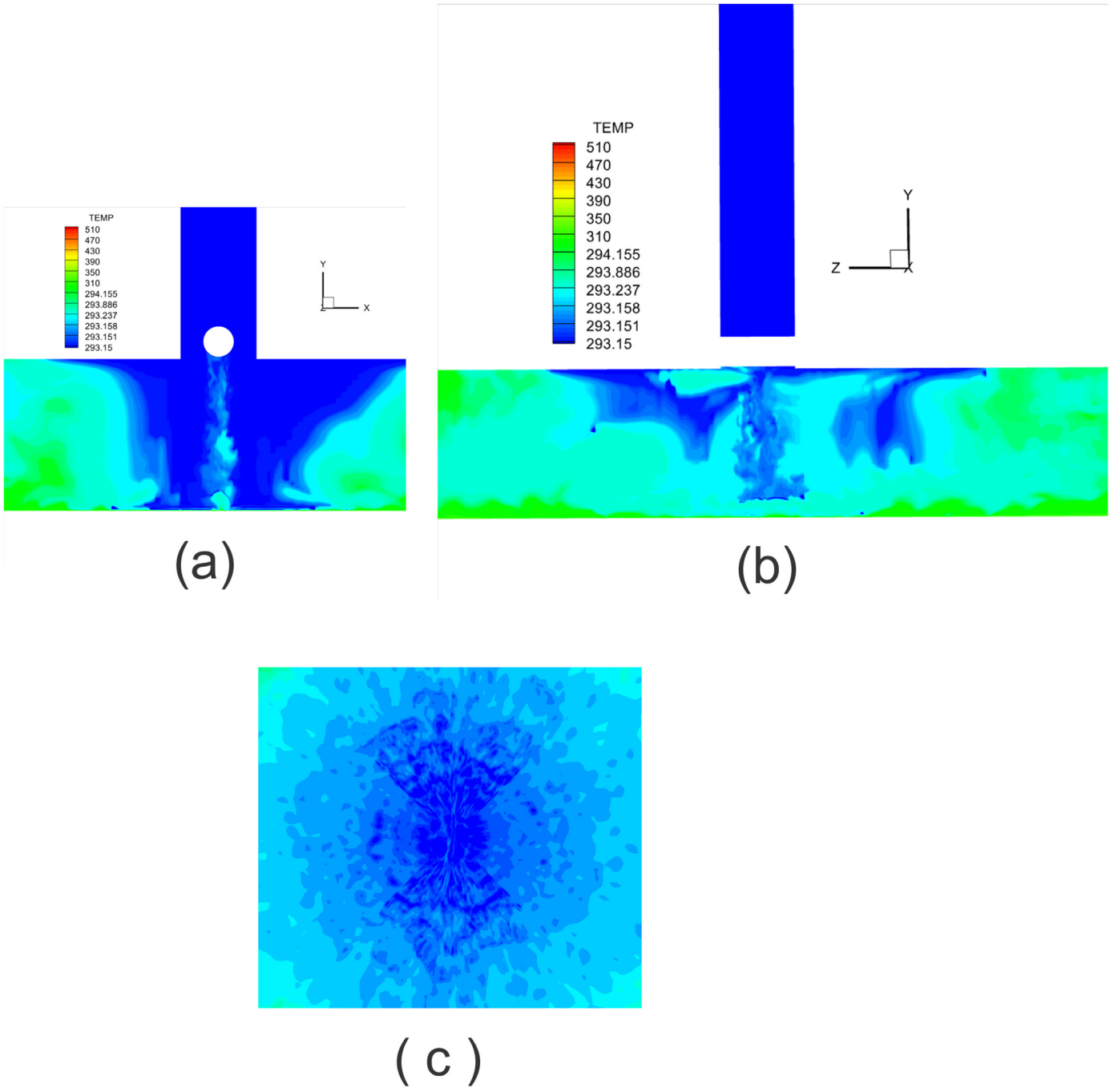

Figure 5. Instantaneous temperature field (a) perpendicular to insert (b) parallel to insert (c) in stagnation region.

erated which are qualitatively in agreement with prescribed turbulent fluctuations. This requires also a prescribed autocorrelation function R_{uu} which defines the homogeneous turbulence levels as developed (see Klein et al. [27]). The autocorrelation function is defined as:

$$R_{uu}(\hat{r}) = \exp\left(\frac{-\pi \hat{r}^2}{4L(t)^2}\right) \tag{9}$$

where, $L(t) = \sqrt{2\pi\nu(t - t_o)}$ is the integral length scale at the inflow plane and $\hat{r}$ is the position vector. According to this procedure, the inflow turbulent velocity generated is based on the relation:

$$u_i = < u_i > + a_{ij} u_j' \tag{10}$$

where, $< u_i >$ is the mean axial velocity, u_j' are velocity fluctuations and a_{ij} is the Cholesky factorization of the Reynolds stress tensor. To accomplish this task a separated LES periodic pipe flow simulation is executed and turbulent fluctuations were used. This approach greatly reduced the computational burden.

Outlet boundary Condition: A convective boundary is specified at the outlet of the domain (Colonius [28]):

$$\frac{\partial U}{\partial t} + K\frac{\partial U}{\partial r} = 0 \tag{11}$$

The quantity K is taken to be a constant mean convection velocity of the large-scale structures.

At the target wall, a constant heat flux per unit area (q_w) of 1,000 W/m^2 is applied. The value of heat flux applied will af-

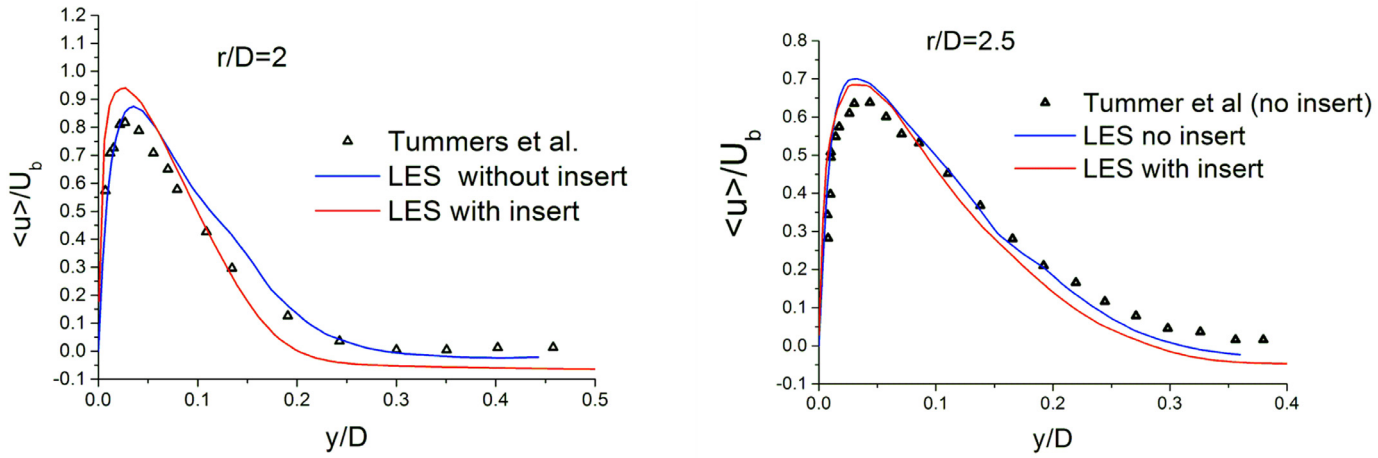

Figure 6. Distribution of time averaged wall jet radial velocity component <u> With and without insert at r/D=2 and 2.5. For the no insert case LES predictions are compared with Tummers et al. data.

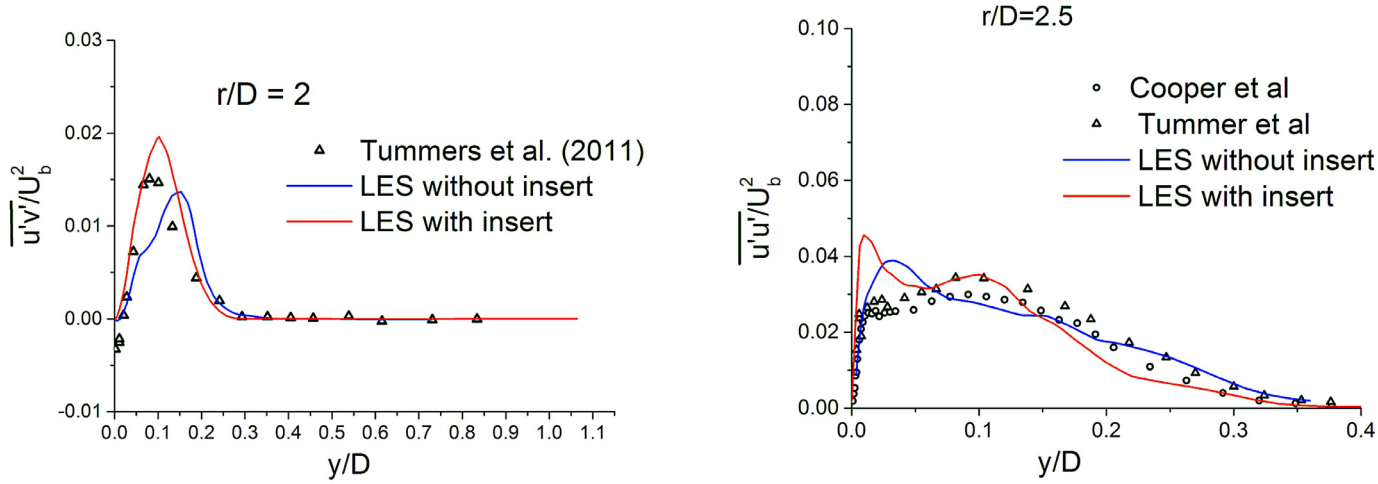

Figure 7. Distribution of time averaged $\overline{u'v'}$ and $\overline{u'u'}$ distribution in wall jet region at r/D = 2 and 2.5 for case of with and without insert. The no insert case LES predictions are compared with Tummers et al. (2011) and Cooper et al data (1993).

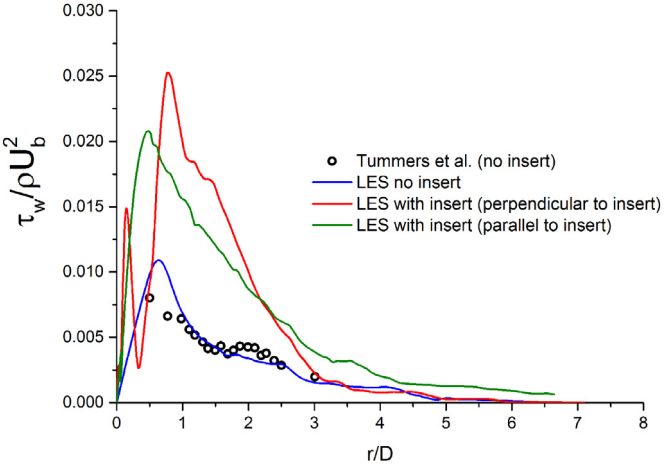

Figure 8. The normalized shear stress is plotted and compared with Tummers et al data.

fect the temperature of jet in stagnation zone and wall-jet development zone. Since the heat transfer is reported in terms of Nusselt number, the value of heat flux applied is not that important.

Adiabatic and no-slip wall boundary conditions are applied at the pipe wall and insert. The boundary condition at the top wall close to jet's outlet is thermally adiabatic and no-slip. The temperature field inside the computational domain is initialized using the jet's inlet temperature which is set to 293 K. The domain is initialized with the same value as the jet's inlet temperature. It is known that the entraining fluid temperature has an influence over the pre-impinged jet's temperature. However, since in current numerical simulations the jet's inlet temperature and entraining fluid temperature near jet are the same, this caused no change in the bulk inlet jet's temperature field.

4. Flow Solver

All computations were executed in non-commercial CFD code called FASTEST (Flow Analysis Solving Transport Equations Simulating Turbulence) (see Sternel [29]). This code is based on finite-volume methods and it solves the three-dimensional filtered Navier-Stokes and energy equations. The sub-grid model proposed by Germano et al. [19] is used in computations reported in this paper. The SIMPLE algorithm is used for pressure velocity coupling. The second order accurate time discretization scheme called implicit Crank-Nicolson method is used. For the space discretization of the convective terms, a second order central differencing scheme

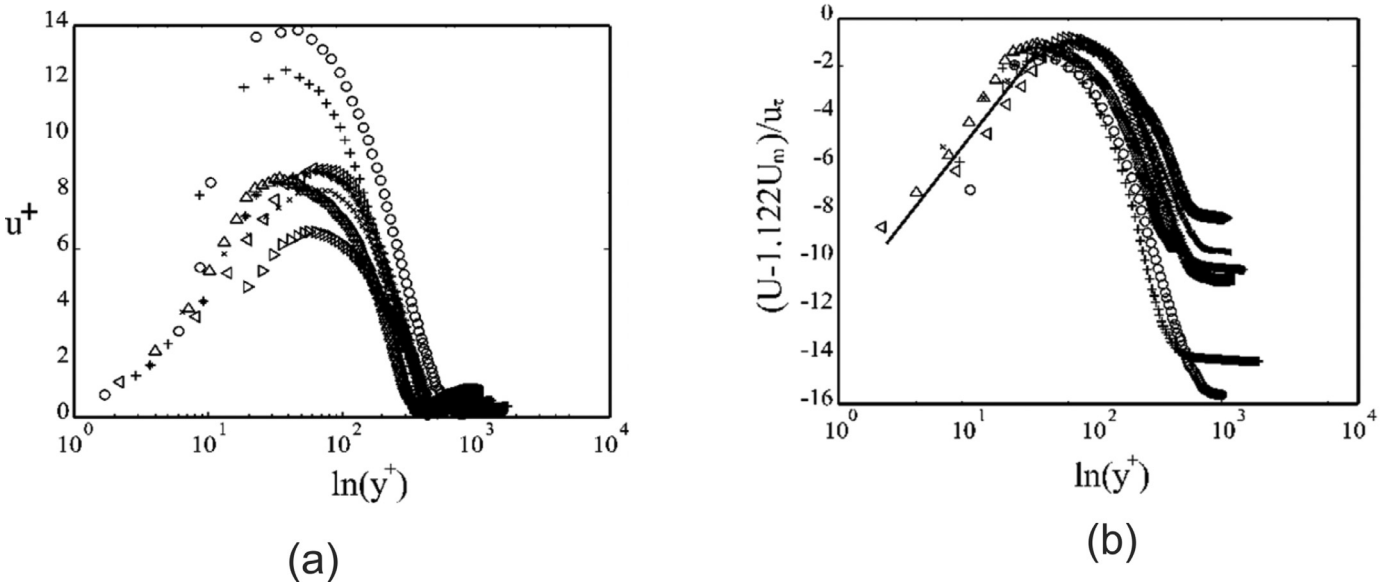

Figure 9. Semi-logarithmic plot of the radial velocity profiles without subtracting the shift parameter, (b) Velocity profile with subtraction of profile shift parameter, the line shows the characteristic of the equilibrium layer that extends till the location of maximum velocity.(Normal to the axis of insert) ◦ r/D=1, + r/D=1.5, * r/D=2, x r/D=2.5, ◄ r/D=3, ▹ r/D=3.5, △ r/D=4.

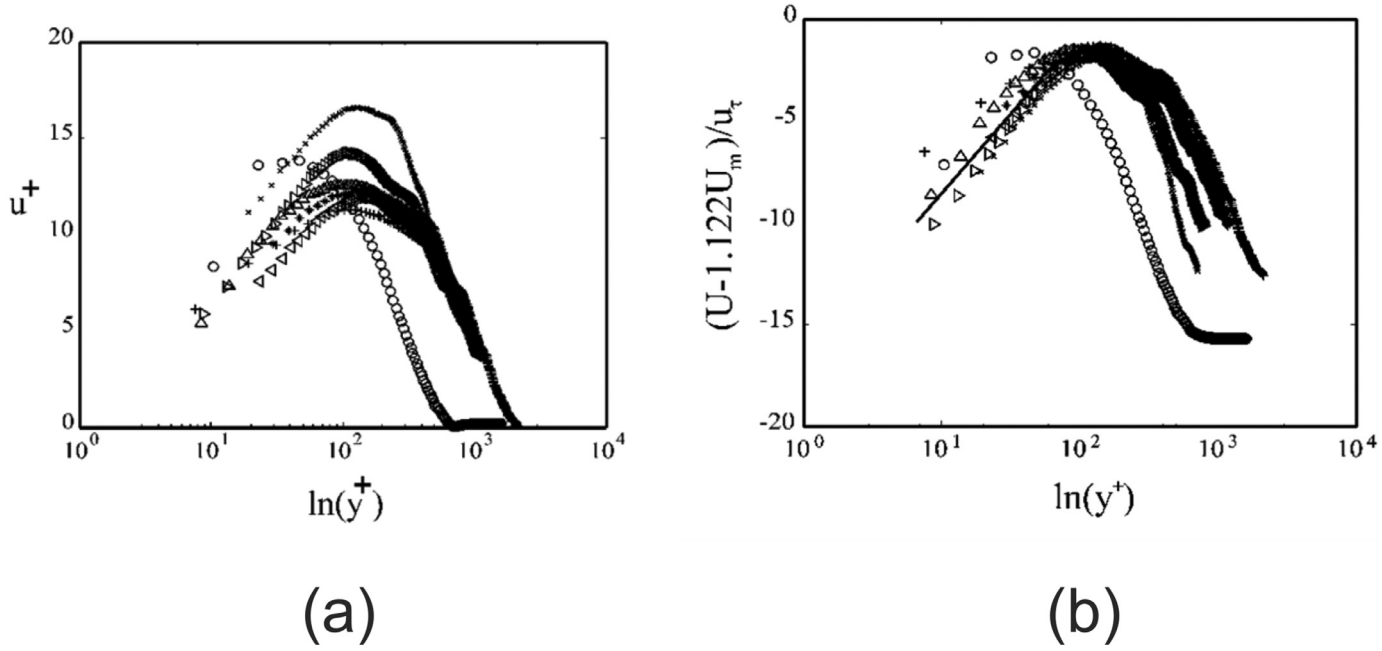

Figure 10. Semi-logarithmic plot of the radial velocity profiles without subtracting the shift parameter, (b) Velocity profile with subtraction of profile shift parameter, the line shows the characteristic of the equilibrium layer that extends till the location of maximum velocity. (Parallel to the axis of insert) ◦ r/D=1, + r/D=1.5, * r/D=2, x r/D=2.5, ◄ r/D=3, ▹ r/D=3.5, △ r/D=4.

is used. The resulting set of equations is solved using the SIP solver [30].

5. Problem Description and Computational Setup

Both the computational domains (Figure 1) are consist of a cylindrical domain and a circular pipe. The case of jet impingement without insert is shown in Figure 1(a). A delivery pipe length (L_p) of 2*D* is used for the no-insert case, whereas, the delivery pipe length (L_p) of 6D is used for the cylindrical insert case. Here *D* is the diameter of the delivery pipe. The diameter of the main impingement region domain connected with the delivery pipe is 16 *D*. The jet issues through the pipe at the centre of the main domain. For both cases, the distance between jet's outlet to the target wall is 2D. The jet Reynolds number, based on *D* and the time averaged bulk velocity $U_{b,}$ is 23,000. The diameter of the cylindrical insert is 0.4 times of the diameter of the main pipe. The center of the cylinder is located at (x,y,z)=(0, 2.2D, 0) in Cartesian coordinates, e.g. 0.2D inside pipe just before the jet issues into main impingement domain.

The whole computational domain is modelled using an O-grid and hexahedral structured cells. The grid was constructed using ICEM-CFD of ANSYS, Inc [31]. The details of grids used in this work are summarised in Table-I. In case of no cylindrical insert in the

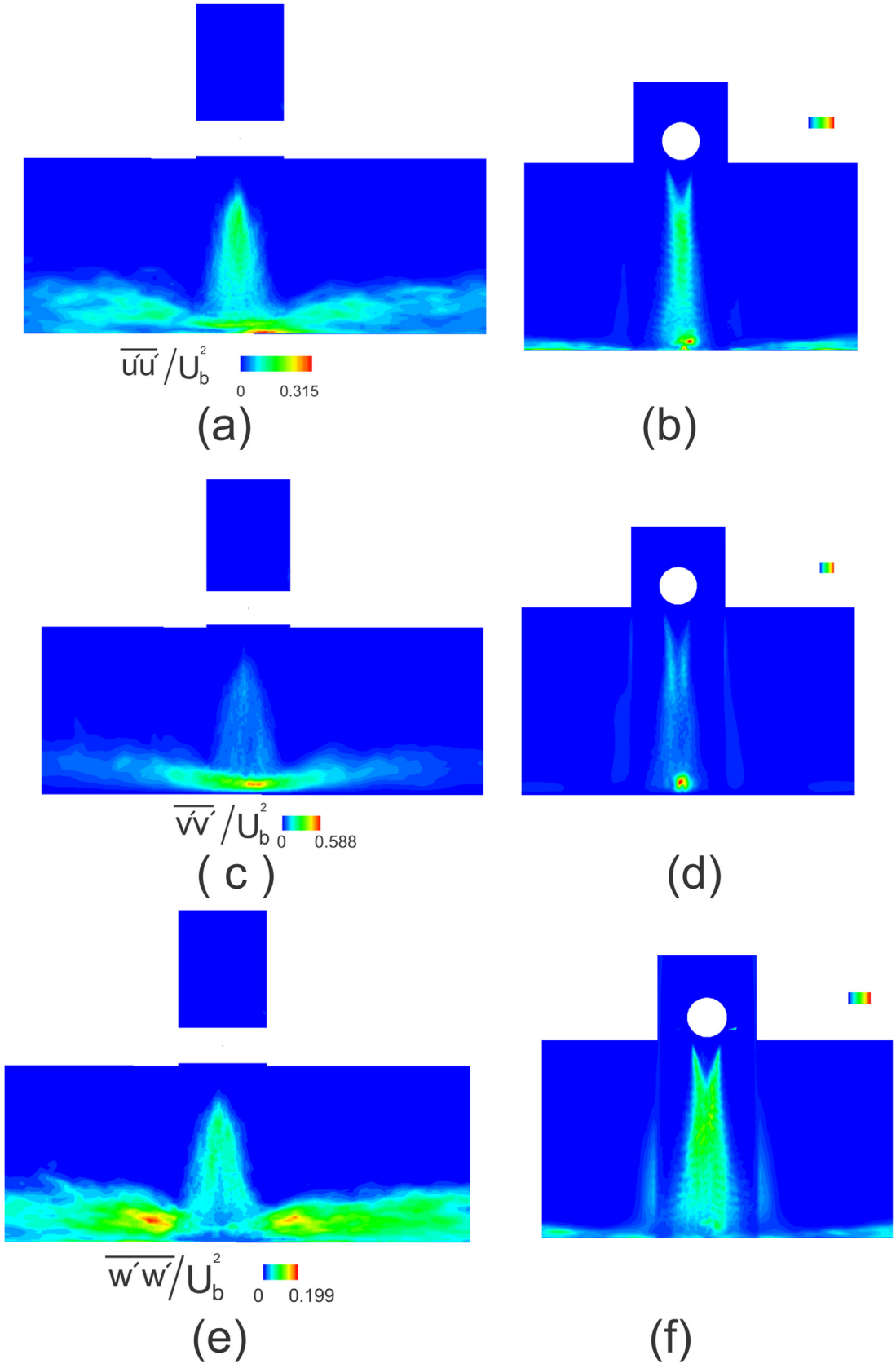

Figure 11. Turbulent velocity fuctuations (a & b) $\overline{u'u'}$ (c & d) $\overline{v'v'}$ (e & f) $\overline{w'w'}$ in the domain in the insert cross section (perpendicular to axis of cylinder) and in the transverse direction (parallel to the axis of insert). The location of highest turbulent kinetic energy is above the stagnation region.

Table 1
Grid Resolution in impingement and starting wall jet zone (r < 4D)

Cases	Jet impingementwithout insert	Jet Impingementwith cylindrical insert
Total Grid Size (Million CV)	10	7.3
Near-wall y^+ value	0.2	0.5
Mean $\Delta r^+ = (\Delta r)u_\tau/\nu$	29	16
Mean $r\Delta\theta^+ = (r\Delta\theta)u_\tau/\nu$	17	20

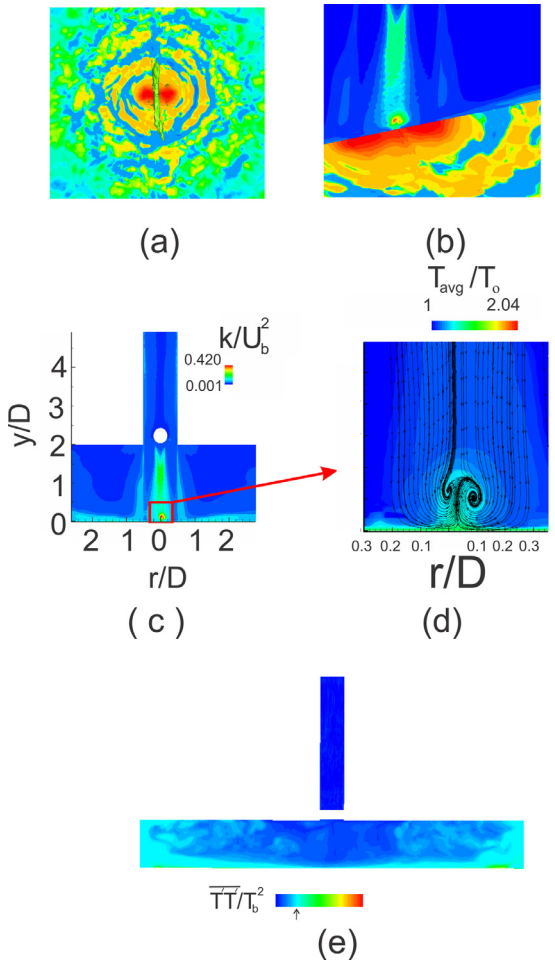

Figure 12. (a) Distribution of turbulent kinetic energy in the impinging jet zone (a) iso-surface of turbulent kinetic energy ($k/U_b^2 = 0.32$) along with pressure distribution at target wall (b) the location of maximum turbulent kinetic energy is shown along with pressure distribution at target wall (c) The location of the near wall plume formation along with turbulent kinetic energy is shown. (d) Time averaged turbulent temperature shows that there is a plume formation in near wall region. (e) Time averaged turbulent temperature fluctuations would increase away from the jet as the wall jet undergo radial spreading.) The arrow on legend indicates the value at the stagnation region which is $\overline{T'T'} = 2$.

pipe, the total grid consist of 10 million control volumes. The dimensionless mean grid spacing $\Delta r^+ = (\Delta r)u_\tau/\nu$ is 29 in radial direction and 16 in azimuthal direction.

Figure 1 (b) shows the computational domain used for the -LES investigation for the case of cylindrical insert at the jet outlet. In the near wall region, the mesh quality fulfils the requirements as deemed necessary for a properly resolved large eddy simulation. The mean mesh spacing near the wall corresponds to $\Delta^+/\eta^+ = 6.4$, where η is the order of the Kolmogorov scale and Δ is grid spacing. The most important region for an impinging jet is the stagnation and wall jet regions. It is known that the for the wall jet region (r/D<4) two peaks in Nusselt number are present. In this zone the grid spacing is defined as $\Delta r^+ = (\Delta r)u_\tau/\nu = 8$ within the jet zone and 16 in the wall jet region. This indicates that the number of control volumes used in the jet impingement zone are high. Also close to cylindrical insert the mesh quality is improved. The structured O-grids are used in regions surrounding the insert with 12 blocks surrounding the cylindrical insert. Overall 7.3 million control volumes were used for the simulation of jet with insert case. The dimension less grid spacing is tabulated in Table 1. During simulations run, the CFL number is maintained at a value less than one. Once flow become statistical stationary, the dimensionless time step $\Delta t d/U_b$ corresponds to $3.57\text{x}10^{-08}$, where d is the diameter of the cylindrical insert. The total simulation time was 90 cycles. The flow took around 20 cycles to attain statistical stationary state. Here one cycle corresponds to the vortex shedding frequency of the cylindrical insert. Once the flow became statistical stationary, it was averaged in time. Also in plots, presented in this paper the flow and thermal fields are averaged at radial positions.

The computations were done in a Cartesian coordinate system. However, as the domain is cylindrical the results are reported along the radius of target wall. Figure 1 (c) shows the radius coordinate used for post-processing of the computational results in the following section. Figure 1(d) shows the plane parallel to the insert axis which is used to extract data later in this paper.

Figure 2 (a) shows the cross section of the gird used for natural jet impingement and Figure 2 (b) shows the grid used for jet impingement with a cylindrical insert. Figure 2 (c) shows the close-up view of the grid surrounding the cylindrical insert.

6. Results and Discussion

In this section, first the mean and instantaneous flow field inside the wall jet region are presented. This is followed by the presentation of the law of the wall for the wall-jet region. After that the turbulent kinetic energy levels are discussed along with anisotropy in the stagnation and wall jet region. Finally the heat transfer from jet impingement is explained.

The placement of the cylinder in the pipe causes the formation of a wake region which extends till the target wall. The size and strength of this wake region changes in time and the vortices shed by the cylinder strike the surface. It has been found experimentally that different vortex structures formed sweeping over the cylinder in wake region leading to different flow topology as outlined in Table 2 (see Lugt [32]). In the context of an external flow over a cylinder, the Reynolds number of the flow, based on the insert diameter, is 11,500. According to Lught [32] for this range of Reynolds number a vortex street with superimposed irregular frequencies is expected. However, here the cylindrical insert is in a confined space and the flow over it is different from free-stream conditions. Lught's [32] flow regimes are for the case of a flow over a cylinder under wind tunnel conditions. The placement of a cylindrical insert inside a pipe and the flow conditions around the cylinder are very different to the free flow around a cylinder in a wind tunnel.

6.1. Mean and Instantaneous flow field

The velocity distributions at the pipe outlet with and without cylindrical insert is shown in Figure 3. Due to the presence of in-

Table 2
Flow over Cylinder (see Lugt[32])

Reynolds number range flow over cylinder	Flow behaviour
$0 < Re_d < 5$	No flow separation
$5 < Re_d < 45$	Vortex pair attached to cylinder
$45 < Re_d < 200$	Purely laminar, vortex street
$200 < Re_d < 4.5 \times 10^5$	Formation of vortex layer; Vortex street superimposed with irregular frequencies
$Re_d > 4.5 \times 10^5$	Turbulent vortex street

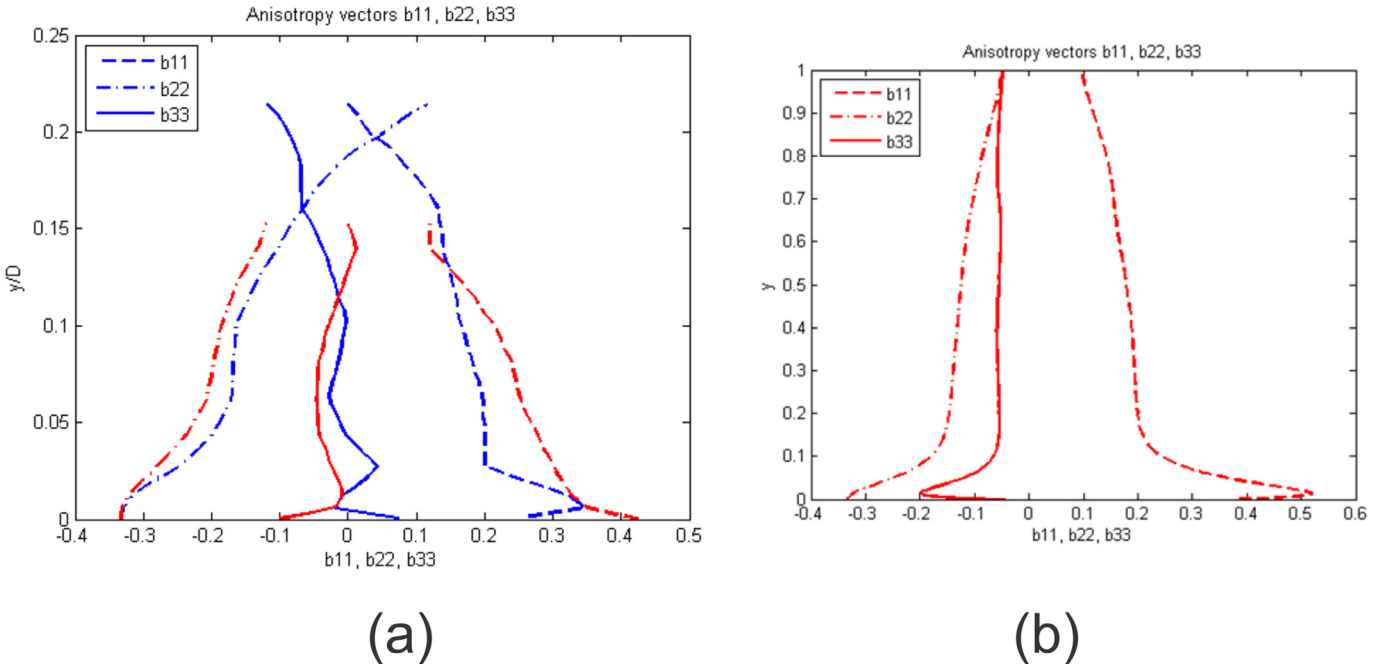

Figure 13. (a) Anisotropy vectors b_{11}, b_{22}, b_{33} for location r/D=2 (blue) and 2.5 (red) in the wall jet region for the case without an insert. (b) Anisotropy vectors from Kim et al. [36] data of channel flow

sert the effective flow region at the jet's outlet is reduced and the mean jet velocity is increased.

Figure 3 shows the velocity distribution inside the jet and the impingement region for both cases. Figure 3 (a) shows the velocity distribution for the case without an insert and Figure 3 (b) shows the time averaged mean velocity perpendicular to the cross-section of the cylinder. Figure 3 (c) shows the time averaged mean velocity in the transverse direction of the cylinder i.e. parallel to the axis of the insert. The flow over the cylindrical insert and the formation of a twin jet system can be identified. In Figure 3(d) the Power Spectral density (PSD) of velocity fluctuations in the jet's shear layer at r=D/2 and y/D=1 is plotted. The line indicates the slope of the inertial subrange. Here k is the wave number. This slope is in agreement with the empirically known characteristics of turbulence spectrum. Also in LES subgrid modelling an important issue is of the energy build up at higher wave numbers. The spectrum confirms the characterstics of Germano model that it does not allow it and thus deemed suitable of thermal and flow analysis.

Figure 4 shows the instantaneous pressure distribution over the target surface. In case of no insert the pressure is highest at the geometric centre of the target wall, as seen in Figure 4 (a). However, for the case of the cylindrical insert the flow is split-up into two parts and the twin jets strike on the target wall creating two distinct high-pressure regions. Figure 4(b) shows the instantaneous pressure distribution at the target wall perpendicular to the cross-section of the cylinder. Figure 4 (c) shows the same distribution in transverse direction of cylinder (parallel to the axis of insert), whereas Figure 4 (d) shows the instantaneous pressure distribution perpendicular to the cylindrical insert. The instantaneous pressure change in the jet's stagnation zone is different from the case with no insert. The insert causes the formation of a high-pressure zone above the insert. Apparently, the similar high pressure is formed over the twin-stagnation zones. This is confirmed through the iso-surfaces of the time averaged pressure field.

Figure 5 (a) shows the instantaneous temperature field perpendicular to the insert whereas figure 5(b) shows the instantaneous temperature field parallel to the insert. Figure 5 (c) shows that the instantaneous temperature distribution at target wall is asymmetric, especially in the stagnation zone due to the twin-jet formation.

Figure 6 shows the distribution of the time averaged wall jet radial velocity component <u> with and without insert at r/D=2 and 2.5. For the case of no insert the predictions are compared with experimental data of Tummers et al. [33]. It can be seen that LES predictions agrees well with experimental data of Tummers et al. [33]. Figure 7 shows the time averaged $\overline{u'v'}$ and $\overline{u'u'}$ distributions in the wall jet region at r/D = 2 and 2.5 for the cases of jet impingement with and without a cylindrical insert.

The case of impinging jet depends a lot on the actual inlet conditions. The information available in the data sets of Cooper et al. [16] and Tummer et al. [33] on the jet's conditions before the outlet is not well elaborated. From experimental data, we can notice that the jet's with the same or close Reynolds numbers can give different Nusselt number distributions (discussed later in the paper). This shows that even through the mean flow is matched in simulations with experimental data the inflow fluctuations are not properly documented.

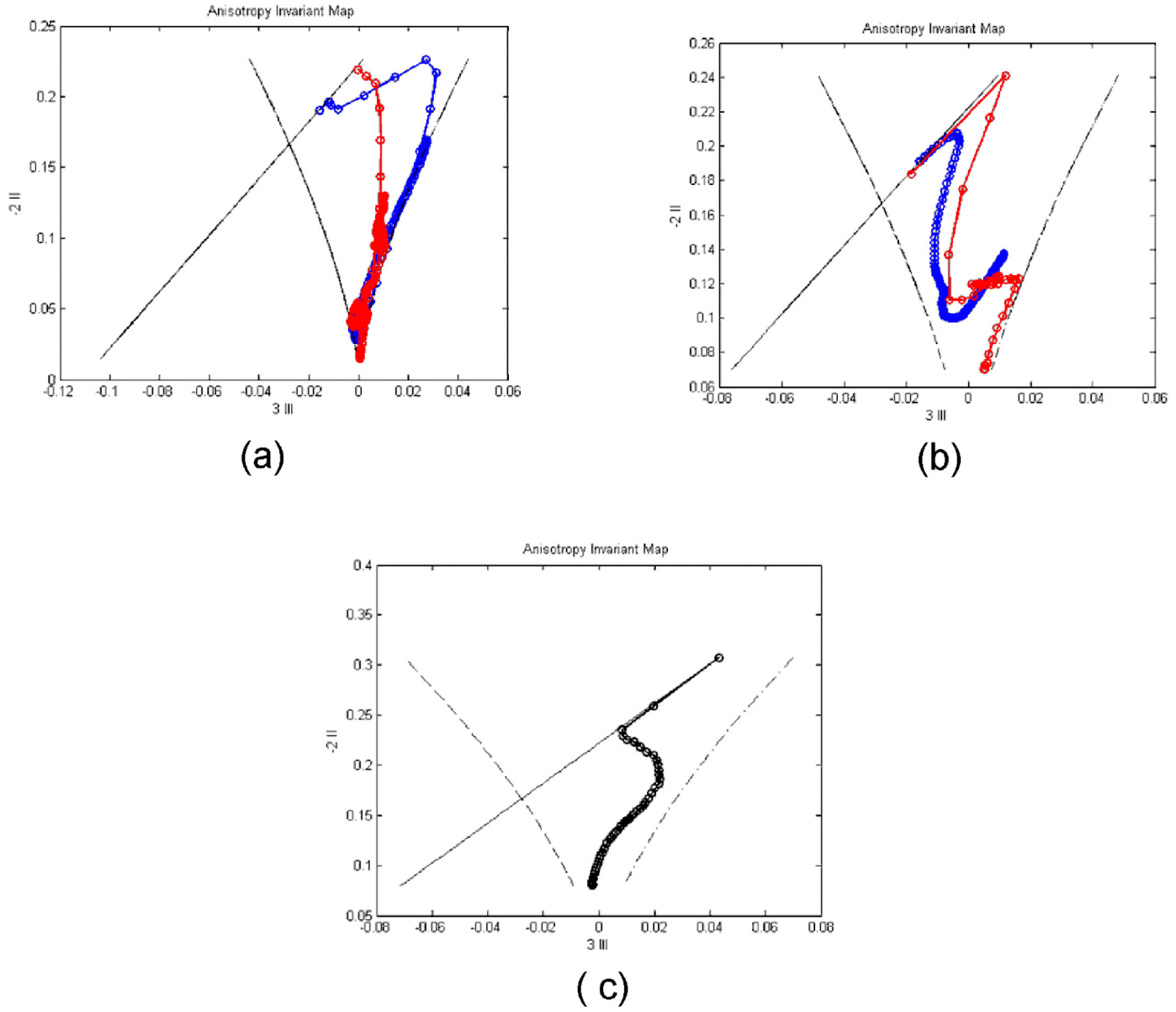

Figure 14. Anisotropy invariant map for location (a) r/D=0.05 (stagnation zone) (b) r/D=2 (wall jet region). The case without an insert is indicated by blue colour and the insert case is indicated in red colour. At r/D=2 the near wall flow is behaving as a two-component type and away from the wall the flow is mainly axisymmetric expansion type. (c) at r/D=2.5 away from wall the flow is in between an axisymmetric expansion and an axisymmetric contraction type.

The LES predictions for the case without insert are also compared with Tummers et al. [33] and Cooper et al. [16] data. The normalized shear stress is plotted in figure 8 and compared with Tummers et al. data [33]. It can be seen that though the order of magnitude of velocity in wall jet region is not very different for both the cases the gradient at the impingement wall is much higher for case of jet impingement with insert than the gradient for case of jet impingement without an insert.

The large velocity gradient in the wall-jet accelerating zone, causes a high skin friction coefficient at the target wall for the jet impingement with insert.

6.2. Law of the wall for the wall-jet region:

Özdemir [34] and Guerra and Feire [35] have investigated the semi-logarithmic wall relation which can be used to model the inner layer inside the wall jet region. They proposed the following relation:

$$u^+ = \frac{u}{u_\tau} = \frac{1}{\kappa}\ln\left(\frac{yu_\tau}{\nu}\right) + B \tag{12}$$

where B is a function of the mean and the the frictional velocity. Using the procedure proposed by Özdemir et al. [34] and Guerra and Feire [35] the following relationship is obtained:

$$B = 1.122\left(\frac{U_m}{u_\tau}\right) - 10 \tag{13}$$

The first term in the above equation is called profile shift parameter, which is subtracted from the law of the wall. The curve obtained represents an equilibrium layer that extends up to the point of the maximum velocity. This has been observed in wall-jet region from experimental investigation for the non-excited jet case [34,35]. Figure 9(a) and 9(b) show the radial velocity profiles in wall jet region with and without subtracting the shift- parameter in semi-logarithmic axes for the velocities normal to the insert axis. Figure 10(a) and 10(b) show the radial velocity profiles with

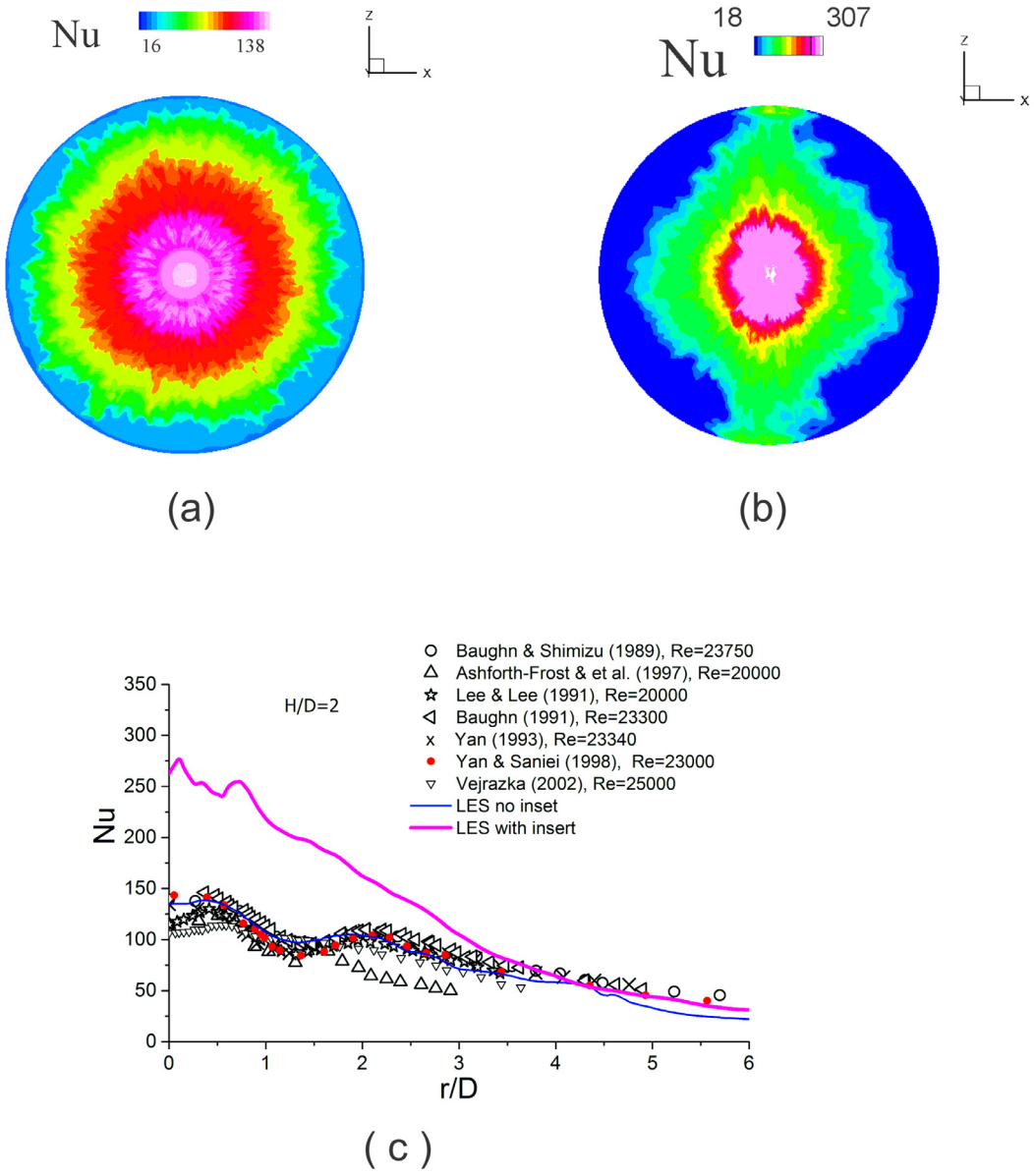

Figure 15. Distribution of Nusselt number at target wall (a) no insert case (b) Asymmetric distribution in case of cylindrical insert. (c) Radial distribution of Nusselt number. Comparison between no-insert and insert case along with experimental validation for the no-insert case.

and without subtracting the shift parameter in semi-logarithmic axes for the velocities parallel to the insert axis in the wall jet direction. It is found that close to impingement zone the flow in wall jet, parallel to the insert axis may deviate from the law of the wall.

6.3. Turbulent Fluctuations

The turbulent kinetic energy is defined as:

$$k = \frac{1}{2}(\overline{u'u'} + \overline{v'v'} + \overline{w'w'}) \tag{14}$$

It is important to understand the benefits of placing an insert in the jet's path. Figure 11 (a & b) show the turbulent velocity fluctuations $\overline{u'u'}$, Figure 11 (c & d) show the turbulent velocity fluctuations $\overline{v'v'}$ and Figure 11 (e & f) show the turbulent velocity fluctuations $\overline{w'w'}$. As seen in the Figure 11 the fluctuations in the target wall normal directions are higher than what has been known for an impinging jet without an insert. In case of regular jet impingement with no inert the radial velocity fluctuations are much higher than the fluctuations normal to a target wall. This confirms that the insert has profound influence on the jet's dynamics and passive excitations leads to changes in fluctuations in the near-wall region.

Figure 12 (a) shows the iso-surfaces of time -averaged turbulent kinetic energy ($k/U_b^2 = 0.32$) close to the target wall while Figure 12 (b) shows distribution of the turbulent kinetic energy in the jet shear layer and in the impingement zone and the location of maximum turbulent kinetic energy which is at y/D=0.12. It is found that the turbulent kinetic energy is maximum in the stagnation zone.

In the case of impingement without insert the location of maximum turbulent kinetic energy is in wall jet region ($k/U_b^2 = 0.054$), whereas in the case of jet impingement with a insert the location of maximum turbulent kinetic energy is within the stagnation zone with the value of ($k/U_b^2 = 0.42$). Comparing the maximum values of turbulent kinetic energies for both the cases there is 670% increase in values of maximum turbulent kinetic energy.

Figure 12 (c & d) shows the close wall plume formation in the stagnation region with time averaged pathlines of time-averaged

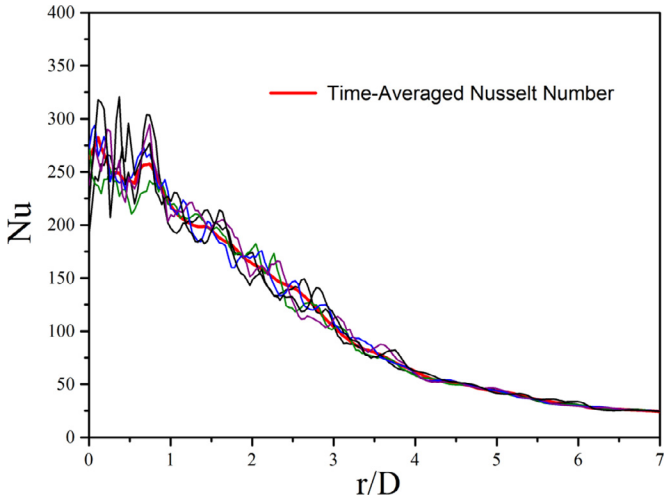

Figure 16. Radially averaged Instantaneous and mean Nusselt number at the target wall (with insert case).

flow field. The time averaged temperature field normalized by the jet's inlet temperature is shown as well. From the time averaged mean flow field it is observed that the plume like region has formed close to the target wall. This happened as the incoming flow from cylindrical insert wake strikes the surface and swept the flow in stagnation region and then created an up-wash region. Although this region is small but the complex flow dynamics has significant influence on the heat transfer. In terms of cylindrical insert's diameter, the location of plume corresponds to a distance of 4.5 times the diameter of insert. It is important to understand that the flow coming from the constricted jet's outlet when impinges on the target wall the flow no longer remains symmetrical. The cumulative dynamics of vortex shedding and flow impingement give rise to asymmetrical flow field in plane of inserts axis and in its normal direction.

Figure 12 (e) shows time averaged turbulent temperature fluctuations in insert transverse direction (Parallel to the axis of insert). These fluctuations in the temperature field are small albeit are present due to wake formation. The arrow at legend indicates the value at the stagnation region which is $\overline{T'T'} = 2$. The time averaged turbulent temperature fluctuations will increase away from the stagnation point as the wall jet become thin due to radial spreading under constant wall heat flux conditions.

6.4. Anisotropy in the stagnation and wall jet region

A plot of anisotropy vectors and the anisotropy invariant map give great insight into turbulent flows, as the invariants do not change with rotation of the coordinate system. This makes them a valuable tool in turbulence analysis. If one component of the velocity fluctuations is larger than the other components than this is called axisymmetric expansion state in anisotropy invariant map, whereas if one component of the velocity fluctuations is smaller than the other two then this is called an axisymmetic contraction state. The anisotropy vectors are defined as:

$$b_{ij} = \frac{\overline{u'_i u'_j}}{2k} - \frac{\delta_{ij}}{3} \tag{15}$$

Where $k = \overline{u'_i u'_i}/2$ represents turbulent kinetic energy δ_{ij} is known as kronecker delta . This gives:

$$b_{11} = \left(\frac{\overline{u'u'}}{2k}\right) - \frac{1}{3}, \quad b_{22} = \left(\frac{\overline{v'v'}}{2k}\right) - \frac{1}{3}, \quad b_{33} = \left(\frac{\overline{w'w'}}{2k}\right) - \frac{1}{3} \tag{16}$$

Figure 13 (a) shows the distributions of the anisotropy vectors b_{11}, b_{22}, b_{33} for the location r/D=2 (blue) and 2.5 (red) in the wall jet region for the case without an insert. Here the streamwise direction of channel flow is compared with the radial wall jet direction. For the sake of comparison, the direct numerical simulation (DNS) data of channel flow from Kim et al. [36] is used and anisotropy vectors are calculated and are plotted in figure 13 (b). The location of r/D=2 & 2.5 is selected as we would like to compare the channel flow with the wall jet region. Most of the turbulence models are designed on data of channel flows. However, the figure 13 shows that the case of impinging jet is very different from the channel flow.

The plot of $-II = b_{ij}b_{ij}/2$ and $III = b_{ij}b_{jk}b_{ki}/3$ is called anisotropy invariant map (AIM) in turbulence literature. Previously Nishino et al. [37] have utilized the anisotropy invariant map (AIM) for the investigation of the nature of turbulence in the stagnation zone of an impinging jet at Reynolds numbers of 10,400 and 13,000 and for a natural jet impingement case. They found that in the stagnation zone the turbulence is following an axisymmetric contraction state close to the wall. Using the present LES data for the jet of Re = 23,000 the anisotropy invariant map for the location r/D=0.05 (stagnation zone) and r/D=2 (in the wall jet region) is plotted in figure 14 (a) and (b) . The case without an insert is indicated by blue colour and the insert case is indicated in red colour. At r/D=2 the near wall flow is behaving as a two-component type and away from wall the flow is mainly in an axisymmetric expansion type. The near wall flow is behaving as a two-component type in both cases. Figure 14 c shows AIM at r/D=2.5. The near wall flow is behaving as a two-component type and away from wall the flow is mainly in an axisymmetric expansion type. At r/D=2.5 away from the wall the flow is in an axisymmetric expansion type. This wall jet behaviour close to wall bounded flow channel data of Kim et al. [36] which predicted two-component behaviour in the near wall region.

6.5. Heat transfer

The Nusselt number is defined as:

$$\overline{Nu} = \left(\frac{-\partial T}{\partial n}\right)_w \left(\frac{D}{\lambda(\overline{T_w} - \overline{T}_j)}\right) = \left(\frac{q''_w}{(\overline{T_w} - \overline{T}_j)}\right)\left(\frac{D}{\lambda}\right) \tag{17}$$

where, λ is thermal conductivity, q''_w is the heat flux $\overline{T_w}$ is the radially averaged temperature attained at the target wall and $\overline{T}_j$ is the mean jet inlet temperature, n indicates the wall normal direction.

Figure 15 shows the distribution of the time-averaged Nusselt number at the target wall. Figure 15 (a) shows the Nusselt number distribution for the case without an insert and Figure 15 (b) shows Nusselt number distribution in the presence of a cylindrical insert. The asymmetric distribution is caused by the twin-jet formation.

Figure 15 (c) shows radially averaged mean Nusselt number at the target wall with and without an insert. Numerical predictions for the case without an insert are compared with experimental data of Baughn and Shimizu [38], Baughn et al. [39], Lee and Lee [40], Yan and Saniei [41], Ashforth-Frost et al. [42], Vejraska [43], Giovannini and Kim [44], Fenot [45].

The radially averaged Instantaneous and mean Nusselt number at the target wall (with insert case) are shown in Fig. 16. It is found that the fluctuations in the Nusselt number distribution are large in the wake region of the cylinder. However, as the wall jet develops the influence of the wake flow is reduced. For the case of a cylindrical insert, the secondary peak in the radial distribution

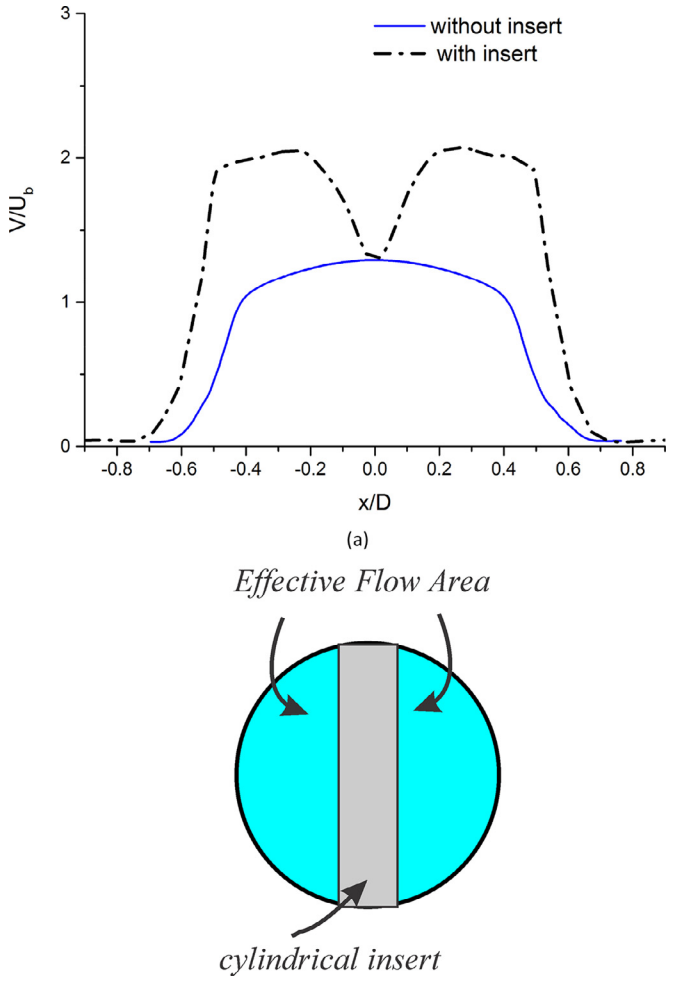

Figure 17. (a) The time averaged mean velocity at a distance of one diameter away from target wall. The data is normalized with bulk inlet velocity. (b) Effective flow area at the location of insert.

of the Nusselt number is found to be shifted towards the zone affected by the wake region. The impact of the high velocity jet streams, originated by the cylindrical insert, causes the increase in heat transfer rates. Due to the cylindrical insert, it is found that two jet streams emerge from the sides of the cylinder with the velocity reaching values twice as high as in the main pipe, causing the Reynolds number to be doubled.

Figure 17 (a) shows the time averaged mean velocity at a distance of one diameter away from the target wall i.e. y/D=1. The velocity is normalized with the bulk velocity at pipe inlet. As can be seen here the inclusion of an insert would cause an increase in velocity of the jet and twin jets are formed. Figure 17 (b) shows the effective flow area as insert is reduced compared with no insert case.

The radial distribution of Nusselt number normalised by $Re^{2/3}$ is plotted in Fig. 18 as suggested by Martin [46]. The Nusselt number is normalised by the Reynolds number of the flow in the main pipe. The Reynolds number based on the hydraulic diameter and the maximum velocity is defined as $Re_{hd} = U_{max}\ D_h/\nu = 12{,}696$, is used for normalization. It is found that as the effective flow area is reduced, this Reynolds number is smaller than the Reynolds number of the flow in the main pipe. The finding that inserts could affect the heat transfer at the target wall has been confirmed by experiments [9]. The current LES simulation results thus support this finding. However, as a word of caution, the authors suggest that

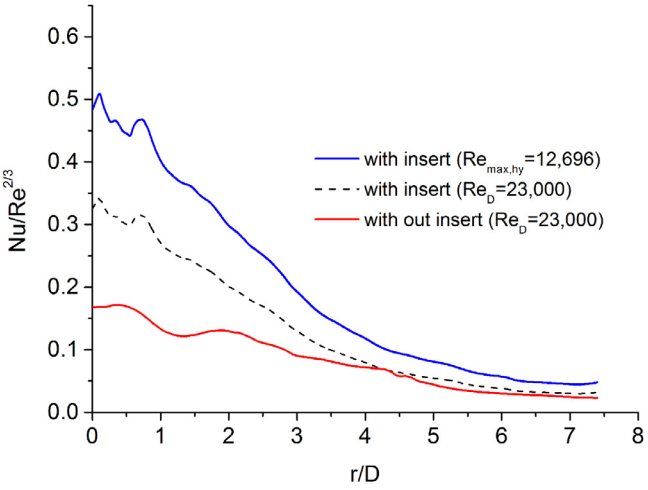

Figure 18. Normalized distribution of radial Nusselt number at target wall.

more experiments are needed to identify optimum insert shapes and flow regimes for heat transfer improvement.

7. Conclusions

The passive excitation of an impinging jet through a cylindrical insert is investigated through LES. The jet is excited passively using a cylindrical insert that is placed just before the jet's outlet. The vortex shedding from the cylinder is changing the flow-filed of the jet. The Reynolds number of the delivery pipe was 23,000 and based on the hydraulic diameter at the insert location and the maximum velocity it is $Re_{hd} = U_{max}\ D_h/\nu = 12{,}696$. The jet's outlet-to-target wall distance is two pipe diameters. Following conclusions can be drawn:

- The presence of an insert will alter the flow and thermal fields of the impinging jet in the stagnation zone, leading to higher skin-friction coefficients and higher heat transfer.
- It can be observed that the insert is causing a departure of the flow behaviour from a free jet and an insert would cause the formation of twin-jets, which velocity twice as high as that of a jet without an insert.
- It is found that the insert can generate flow fluctuations which enhances the heat transfer rates. The time averaged mean flow field shows an up-wash with plume like appearance is generated in the impingement zone in near wall region. It is found that turbulent kinetic energy is very high in this region. Also, the secondary peak in radial distribution of the Nusselt number is found to be shifted towards the impingement zone.
- It is found that the heat transfer is greatly enhanced by the use of such a device.
- The anisotropies generated in the impingement zone are quite different from the channel flow. However, the flow would come closer to channel flow in wall jet development zone.

Declaration of Competing Interest

The authors declare that they have no known competing financial interests or personal relationships that could have appeared to influence the work reported in this paper.

CRediT authorship contribution statement

Naseem Uddin: Methodology, Software, Software, Visualization, Validation, Writing - original draft, Writing - review & edit-

ing. **Sven Olaf Neumann:** Supervision, Writing - review & editing. **Bernhard Weigand:** Conceptualization, Supervision, Writing - review & editing. **Bassam A. Younis:** Conceptualization, Supervision, Writing - review & editing.

Acknowledgement

The authors would like to thank Prof. Dr. M. Schäfer and Dr.-Ing. D. Sternel, (Fachgebiet für Numerische Berechnungsverfahren im Maschinenbau (FNB), Technische Universität, Darmstadt, Germany) for providing the FASTEST code and helpful discussions. Also we would like to thank Mr. Bernd Brasas, ANSYS Inc, Germany for guiding in grid generation. We would like to thank staff of Höchstleistungsrechenzentrum (HLRS), Stuttgart, Germany for organising NEC SX8 cluster used for computations.

References

[1] K. Jambunathan, E. Lai, M.A. Moss, B.L. Button, A review of heat transfer data for single circular jet impingement, Int. J. Heat and Fluid Flow 13 (2) (1992) 106–115 https://doi.org/10.1016/0142-727X(92)90017-4.
[2] R. Viskanta, Heat transfer to impinging Isothermal Gas and Flame jets, Exp. Thermal and Fluid Sciences 6 (1993) 111–134 https://doi.org/10.1016/0894-1777(93)90022-B.
[3] Bernhard Weigand, Sebastian Spring, Multiple Jet Impingement- A Review September 2009, Heat Transfer Research 42 (2) (2009), doi:10.1615/HeatTransRes.v42.i2.30.
[4] C. Gau, W.Y. Sheu, C.H. Shen, Impingement cooling ow and heat transfer under acoustic excitations, Journal of Heat Transfer 119 (1997) 810–817, doi:10.1115/1.2824187.
[5] S.D. Hwang, H.H. Cho, Effects of acoustic excitation positions on heat transfer and flow in axisymmetric impinging jet: main jet excitation and shear layer excitation, International Journal of Heat and Fluid Flow 24 (2003) 199–209 https://doi.org/10.1016/S0142-727X(02)00236-9.
[6] P. Jiang, Y.C. Guo, C.K. Chan, W.Y. Lin, Frequency characteristics of coherent Structures and their excitations in small aspect-ratio rectangular jets using large eddy simulations, Computers & Fluids 36 (2007) 611–621, doi:10.1016/j.compfluid.2006.05.001.
[7] N. Uddin, Turbulence modeling of complex flows in CFD, University Stuttgart, Germany, 2008 PhD thesis.
[8] H. Herwig, H. Mocikat, Gürtler, S. Göppert, Heat transfer due to unsteadily impinging jets, Int. J. of Thermal Sciences 43 (2004) 733–741, doi:10.1016/j.ijthermalsci.2004.02.013.
[9] Yoshiaki Haneda, Yoshiaki Tsuchiya, Hideo Kurasawa, Kazuyoshi Nakabe, Kenjiro Suzuki, Flow field and heat transfer of a two-dimensional impinging jet disturbed by an elastically suspended circular cylinder, Heat Transfer - Asian Research 30 (4) (June 2001) 313–330, doi:10.1002/htj.1020.
[10] N. Gao, H. Sun, D. Ewing, Heat transfer to impinging round jets with triangular tabs, International Journal of Heat and Mass Transfer 46 (14) (2003) 2557–2569 https://doi.org/10.1016/S0017-9310(03)00034-6.
[11] S. Bhattacharya, A. Ahmed, A note on unsteady impinging jet heat transfer, Experimental Thermal and Fluid Science 34 (2010) 633–637, doi:10.1016/j.expthermflusci.2009.12.004.
[12] Y. Li, Q. Lin, Z. Zhu, LES of normally impinging elliptic air-jet heat transfer at Re=4400, Advances in Applied Mathematics and Mechanics 9 (2) (2017) 485–500, doi:10.4208/aamm.2015.m1078.
[13] T. Natarajan, J. Jewkes, A.D. Lucey, R. Narayanaswamy, Y.M. Chung, Large eddy simulations of a turbulent jet impinging on a vibrating heated wall, International Journal of Heat and Fluid Flow 65 (2017) 277–298 https://dx.doi.org/10.1016/j.ijheatfluidflow.2016.11.006.
[14] B. Krumbein, S. Jakirlić, C. Tropea, VLES study of a jet impinging onto a heated wall, International Journal of Heat and Fluid Flow 68 (2017) 290–297, doi:10.1016/j.ijheatfluidflow.2017.09.020.
[15] P.S. Penumadu, A.G. Rao, Numerical investigations of heat transfer and pressure drop characteristics in multiple jet impingement system, Applied Thermal Engineering 110 (2017) 1511–1524 https://doi.org/10.1016/j.applthermaleng.2016.09.057.
[16] D. Cooper, D.C. Jackson, B.E. Launder, G.X. Liao, Impinging jet studies for turbulence model assessment- I. Flow field experiments, Int. J. Heat Mass Transfer 36 (10) (1993) 2675–2684, doi:10.1016/S0017-9310(05)80204-2.
[17] N. Uddin, S.O. Neumann, B. Weigand, LES simulations of an impinging jet: On the origin of the second peak in the Nusselt number distribution, International Journal of Heat and Mass Transfer 57 (2013) 356–368, doi:10.1016/j.ijheatmasstransfer.2012.10.052.
[18] S.B. Pope, Turbulent Flows, Cambridge University Press, United Kingdom, 2000.
[19] M. Germano, U. Piomelli, P. Moin, W.H. Cabot, A dynamic subgrid-scale eddy viscosity model, Phys. Fluid A 3 (7) (1991) 1760–1765, doi:10.1063/1.857955.
[20] J.W. Deardorff, Three dimensional numerical modeling of planetary boundary layer, in: Duane A. Haugen (Ed.), Workshop on Micrometerology, Chapter 7, 271-311, Am. Meteorol. Soc., In book: Workshop on Micrometeorology, 1973.
[21] J.W. Deardorff, Stratocumulus-capped mixed layers derived from a threedimensional model, Boundary layer Meterorol. 32 (1980) 205–236, doi:10.1007/BF00119502.
[22] C.H. Moeng, J.C. Wyngaard, Spectral analysis of large eddy simulations of convective boundary layers, J, Atmos. Sci Vol. 45 (23) (1988) 3573–3587, doi:10.1175/1520-0469(1988)045⟨3573:SAOLES⟩2.0.CO;2.
[23] S. Gao, D.C. Leslie, P.R. Voke, Large eddy simulation of thermal impinging jets, Rep ME-FD/91.02 Dep. Mech. Eng., University of Surrey, Guildford, UK, 1991.
[24] M. Hadziabdic, LES, RANS and Combined Simulation of Impinging Flows and Heat Transfer, TU Delft, 2005 PhD. Thesis.
[25] W.M. Kays, M.E. Crawford, B. Weigand, Convective Heat and Mass Transfer, McGraw-Hill, 2004.
[26] F.M. White, Fluid Mechanics, 7th ed, Mcgraw-Hill series in mechanical engineering, 2009 ISBN 978–0–07–352934–9.
[27] M. Klein, A. Sadiki, J. Janicka, A digital filter based generation of inflow data for spatially direct numerical or large eddy simulations, Journal of computational Physics 18 (2003) 652–665, doi:10.1016/S0021-9991(03)00090-1.
[28] T. Colonius, Numerically non-reflecting boundary and interface conditions for compressible ow and aeroacoustic computations, J. AIAA 35 (7) (1997) 1126–1133, doi:10.2514/2.235.
[29] D. Sternel, FASTEST, User Manual, Department of Numerical Methods in Mechanical Engineering, Technische Universität Darmstadt, 2005.
[30] H.L. Stone, Iterative solution of implicit approximations of multidimensional partial differential equations, SIAM J. Numer. Anal. 5 (1988) 530–558, doi:10.1137/0705044.
[31] ANSYS ICEM CFD, http://www.ansys.com/products/icemcfd.asp.
[32] H. Lugt, Vortex flows in Nature and Technology, Wiley & Sons, 1983.
[33] M.J. Tummers, J. Jacobse, S.G.J. Voorbrood, Turbulent flow in the near field of a round impinging jet, Int. J. Heat Mass Transfer 54 (2011) 4939–4948, doi:10.1016/j.ijheatmasstransfer.2011.07.007.
[34] I.B. Özdemir, J.H. Whitelaw, Impingement of an axis-symmetric jet on unheated and heated at plates, J. Fluid Mech. 240 (1992) 503–532 https://doi.org/10.1017/S0022112093003854.
[35] D.R.S. Guerra, J. Su, A.P.S. Feire, The near wall behaviour of an impinging jet, Int. J. Heat and Mass Transfer 48 (2005) 2829–2840, doi:10.1016/j.ijheatmasstransfer.2005.01.027.
[36] J. Kim, P. Moin, R. Moser, Turbulence statistics in fully developed channel flow at low Reynolds number, Journal of Fluid Mechanics 177 (April 1987) 133–166, doi:10.1017/S0022112087000892.
[37] K. Nishino, M. Samada, K. Kasuya, K. Torii, Turbulence statistics in the stagnation region of an axisymmetric impinging jet flow, Int. J. Heat Fluid Flow 17 (1996) 193–201, doi:10.1016/0142-727X(96)00040-9.
[38] J.W. Baughn, S. Shimizu, Heat Transfer Measurement from a Surface with Uniform Heat Flux, and an Impinging Jet, Int. J. Heat Transfer 111 (1989) 1096–1098, doi:10.1115/1.3250776.
[39] W.J. Baughn, A.E. Hechanova, X. Yan, An Experimental Study of Entrainment Effects on the Heat Transfer from a at Surface to a Heated Circular Impinging Jet, J. Heat Transfer 113 (1991) 1023–1025, doi:10.1115/1.2911197.
[40] J. Lee, S. Lee, Stagnation Region Heat Transfer of a Turbulent Axisymmetric Jet Impingement, Exp. Heat Transfer 12 (1999) 137–156, doi:10.1080/089161599269753.
[41] X. Yan, N. Saniei, Heat Transfer Measurements From a Flat Plate to a Swirling Impinging Jets, Pro. 11th Int. Heat Transfer Conference, 1998, doi:10.1615/IHTC11.2320.
[42] S. Ashforth-Frost, K. Jambunathan, C.F. Whitney, S.J. Ball, Heat transfer from a flat plate to a turbulent axisymmetric impinging jet, Proc. Instn. Mech. Engrs. 211 (Part C) (1997) 167–172, doi:10.1243/0954406971521746.
[43] J. Vejrazka, Experimental study of pulsating round impinging jet PhD Thesis, Institute of Chemical Process Fundamentals, Prague, 2002.
[44] A. Giovannini, N.S. Kim, Impinging jet: Experimental analysis of fluid field and heat transfer for assesment of turbulent models, Annals of the Assembly for Int. Heat Transfer Conference 13, TRB-15, 2006, doi:10.1615/IHTC13.p1.150.
[45] M. Fenot, Etude du refroidissement par impact de jets. application aux aubes de turbines, Université de Poitiers, France, 2004.
[46] H. Martin, Heat and mass transfer between impinging gas jets and solid surfaces, Adv. Heat Transfer 13 (1977) 1–60, doi:10.1016/S0065-2717(08)70221-1.